SAND2016-14160C

Combined Effects of Fuel and Dilution Type on Efficiency Gains of Lean Well-Mixed DISI Engine Operation with Enhanced Ignition and Intake Heating for Enabling Mixed-Mode Combustion

Magnus Sjöberg and Wei Zeng
Sandia National Laboratories

Abstract

Well-mixed lean or dilute SI engine operation can provide efficiency improvements relative to that of traditional well-mixed stoichiometric SI operation. However, the realized gains depend on the ability to ensure stable, complete and fast combustion. In this work, the influence of fuel type is examined for gasoline, E30 and E85. Several enabling techniques are compared. For enhanced ignition stability, a multi-pulse (MP) transient plasma ignition system is compared to a conventional high-energy inductive spark ignition system. Combined effects of fuel type and intake-gas preheating are examined. Also, the effects of dilution type (air or N_2-simulated EGR) on lean efficiency gains and stability limits are clarified. The largest efficiency improvement is found for lean gasoline operation using intake preheating, showing the equivalent of a 20% fuel-economy gain relative to traditional non-dilute stoichiometric operation. The reason for gasoline's larger efficiency improvement is its lower octane number which facilitates the use of end-gas autoignition to produce mixed-mode combustion. For these conditions, such mixed-mode combustion is required for rapid completion of the inherently slow lean combustion event prior to piston expansion. The fuel-economy gains are somewhat smaller for both E30 and E85 because of higher resistance to end-gas autoignition under lean conditions.

To avoid knocking cycles when mixed-mode combustion is used, the deflagration-based combustion must be very repeatable to ensure consistent compression of the end-gas reactants. Multi-pulse transient plasma ignition is used beneficially to stabilize the combustion, especially for dilute operation which suffers from low flame speeds. However, even with an enhanced ignition system, the best fuel-economy gains of dilute stoichiometric operation with mixed-mode combustion are on the order of 11-12%, which is substantially less than for lean operation.

INTRODUCTION

Climate change [1] and the need to secure energy supplies are two reasons for a growing interest in engine efficiency and alternative fuels. Well-mixed stoichiometric operation is the dominating combustion mode for gasoline SI engines used for automotive applications. It allows cost-effective compliance with stringent exhaust emissions regulations by the application of a three-way catalyst for reduction of NO_x and oxidation of CO and HC [2]. However, there are several reasons why stoichiometric operation (without exhaust-gas recirculation, EGR) limits the observed engine efficiency, especially for low and intermediate loads. First, the required intake throttling results in pumping losses. Second, high combustion temperatures lead to both high heat-transfer losses and unfavorable thermodynamic properties of the combustion products. The latter manifests itself as high specific heat capacity, reducing the ratio of specific heats (γ) which leads to a reduction of the work-extraction efficiency of the expansion stroke [2]. A third factor is the inability of the stoichiometric combustion to fully complete near TDC due to dissociation of CO_2 in the hot O_2-depleted gases [3,4].

Fuel-lean operation can improve engine efficiency by reducing all of these effects. However, the challenge is to maintain stable and efficient combustion despite a reduction of flame speeds in fuel-lean mixtures [5]. The reduction of flame speeds becomes a particular problem from the perspective of ignition and effective flame spread throughout the charge. A recent study demonstrates the combined benefits of intake gas heating and multi-pulse (MP) transient plasma-ignition on lean stability limits for a blended fuel of gasoline with 85% ethanol by volume (E85) [6]. Even a moderate 40K increase of the in-cylinder charge temperature at intake valve closing (IVC) provided a significant extension of the lean-stability limit from a fuel/air equivalence ratio (ϕ) of 0.56 down to 0.51. Using the MP ignition system, the lean-stability limit was extended further down to ϕ = 0.49. High-speed plasma and flame imaging revealed that the MP ignition system provided a much faster transition from ignition to fully developed turbulent combustion [6].

Although previous studies have provided useful information on lean-stability limits [2,5-11], systematic experiments among fuels and fuel blends in the same facility are needed to provide quantitative comparisons. Furthermore, stoichiometric operation with dilution is also of interest, because it can provide fuel-economy benefits while allowing the use of a cost-effective three-way catalyst for NO_x reduction. This study extends previous work [6], examining new data acquired with both 100% gasoline and a blend of gasoline with 30% ethanol by volume (E30), while including comparisons with existing data for E85. In addition to lean operation, the current study also examines N_2-diluted stoichiometric operation that simulates operation with EGR. The current study also offers new insights by systematically comparing engine operation with two different fuels at two intake temperatures and with two dilution types. In addition, the MP ignition system is used to probe the limits and characteristics of lean and dilute SI combustion beyond what is possible with conventional inductive spark systems.

There are two main objectives. First, to reveal effects of fuel type and octane number on the efficiency of lean or dilute SI operation. Second, to determine viable paths for stable and more efficient lean SI operation.

Experimental Setup

Research Engine Facility

The engine used for the experiments is a single-cylinder four-valve research engine that can be set up in two configurations: an all-metal configuration for continuously fired performance testing, or in a nearly identical optical configuration for imaging studies. All tests here were conducted with the all-metal configuration, using a water-cooled metal cylinder and oil-lubricated metal piston rings. The piston has a moderately deep piston bowl to aid the stratification of fuel for spray-guided stratified-charge operation, *e.g.* Ref. [12]. However, for these tests the fuel was injected during the intake stroke to generate a well-mixed charge. Figure 1 shows a cross section of the combustion chamber with the piston at TDC. The long-reach spark plug allows the spark plasma to develop in a central location of the combustion chamber, which should be particularly beneficial for lean operation. This long-reach spark plug is used with a high-energy inductive ignition system, as described below.

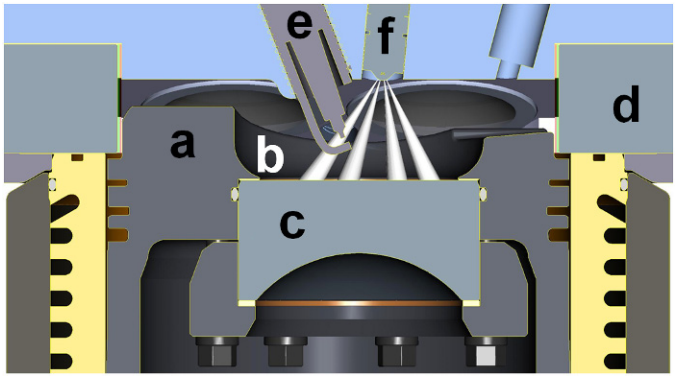

Figure 1. Cross-section of combustion chamber at TDC: a - piston, b - piston bowl, c - piston-bowl window, d - pent-roof window, e - spark plug, and f - fuel injector. Metal window blanks were used in this study.

Engine data are given in Table 1. The engine was fueled using a Bosch 8-hole step-hole VCO injector. The injector was oriented such that two of the fuel sprays straddled the spark-plug gap of the commercial long-reach spark plug. For all data, the phasings of the cam shafts relative to the crank shaft were maintained constant. The cam shafts were phased to provide both low residual levels and high volumetric efficiency. A graphical representation of the valve lifts can be found in Ref. [6]. It should be noted that one intake valve was deactivated to increase in-cylinder swirl and tumble levels, see Table 1. In this study, the crank angles (CA) are referenced as after top dead center of the combustion stroke, aTDC.

The air was metered into the intake system using a sonic-flow nozzle. For the stoichiometric dilute test cases, N_2 was also metered with another sonic-flow nozzle to simulate the reduction of oxygen concentration associated with the use of EGR.

Table 1. Engine Specifications

Displacement	0.552 liters
Bore	86.0 mm
Stroke	95.1 mm
Connecting Rod Length	166.7 mm
Geometric Compression Ratio	12:1
Intake Valve Diameter	35.1 mm
Intake Valve Angle Relative Cylinder Axis	18°
Exhaust Valve Diameter	30.1 mm
Exhaust Valve Angle Relative Cylinder Axis	16°
Swirl / Tumble Index (one intake valve deactivated)	2.7 / 0.62
Fuel Injector	Bosch 8-hole solenoid-type
Hole Orientation	Symmetric with 60° included angle
Hole Size	Stepped-hole, min. dia. = 0.125 mm

In discussions that involve only lean operating points, the traditional fuel/air-equivalence ratio (ϕ) is used to quantify the stoichiometry of the supplied reactants. To aid comparisons of lean and dilute data sets, a mass-based equivalence ratio, ϕ_m, is used:

$$\phi_m \equiv \frac{\left(F/C\right)_{Actual}}{\left(F/A\right)_{Stoichiometric}} \qquad (1)$$

where F = Fuel mass, A = Air mass, and C = gas Charge mass.

In this study with simulated EGR, the gas charge mass equals that of air and N_2, (C = A + N_2 mass). ϕ_m is a measure of the chemical energy per reactant mass, regardless of type of diluent. Hence, the use of ϕ_m allows plotting results from both lean and dilute stoichiometric data sets against the same x-axis. It should be noted that when only air is used as a diluent, $\phi = \phi_m$.

The exhaust gas flow was diluted with extra air using nozzles at the entry point of the exhaust tank. This was done to limit the exhaust gas temperature in the tank and to lower the dew point of the exhaust gases to avoid loss of unburned hydrocarbons (HC) and water due to condensation in the unheated sample lines. With precisely known exhaust dilution, the measured exhaust composition was back-corrected to engine-out mole fractions. A Horiba MEXA-584L emission analyzer measured CO, CO_2 and HC. O_2 was measured with a CAI 600PP gas analyzer. NO_x was measured with a CAI 600CLD gas analyzer. Exhaust smoke was measured with an AVL 415S smoke meter.

To compute a metric of combustion efficiency (η_{comb}), the measured mole fractions of CO and HC were converted to mg/cycle and multiplied with the respective specific lower heating values (LHV):

$$\eta_{comb}\,[\%] = 100 \cdot \frac{\left(m_{Injected-Fuel} - m_{HC}\right) \cdot LHV_{Fuel} - m_{CO} \cdot LHV_{CO}}{m_{Injected-Fuel} \cdot LHV_{Fuel}} \qquad (2)$$

Here, it is assumed that the LHV of the unburned HC equals that of the injected fuel. Further, the contribution from H_2 to combustion inefficiency is neglected since the level of H_2 in the exhaust was not measured. However, the error introduced is small since H_2 emissions only become significant for rich combustion [4]. In this study, focus is on stoichiometric or lean operation.

Ignition Systems

Two ignition systems were used as described in the following.

Regular Inductive System

The conventional inductive system was supplied by Bosch. The spark coil (model ZS-L 1x1E) can provide relatively high spark energy. For all the tests reported here, the charging time of the primary coil was set to 5 ms. According to measurements by Bosch, this results in a spark energy of nominally 106 mJ being delivered from the secondary high-voltage coil. The secondary coil was connected to an NGK spark plug featuring a long-reach single-point J-gap. The spark gap width was adjusted to 1.0 mm prior to the engine tests. A photo of the spark plug is provided in Fig. 2b (bottom).

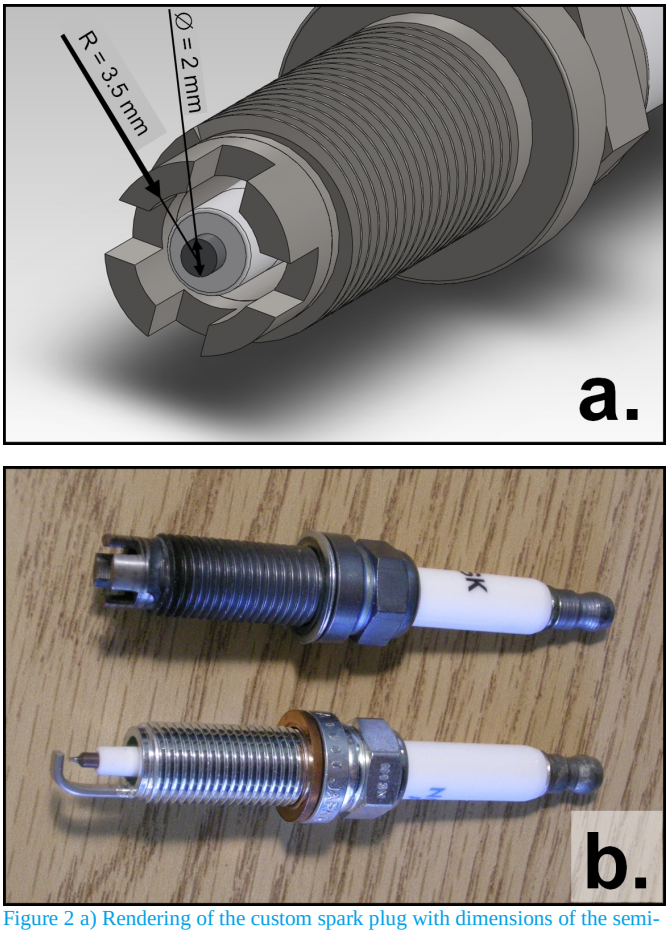

Figure 2 a) Rendering of the custom spark plug with dimensions of the semi-open cavity. b) Photo of the commercial long-reach spark plug (bottom) and the in-house modified spark plug (top).

Enhanced Ignition System

A research-grade advanced ignition system capable of multiple ultra-short pulses was used together with an in-house developed spark plug featuring a semi-open ignition cavity. Figure 2b shows a photo of the custom spark plug (top) in comparison with the commercially available long-reach spark plug (bottom). Figure 2a provides two of the key dimensions of the semi-open ignition cavity. The gap distance from the central positive anode to any of the four wide ground cathodes is 2.5 mm.

The pulse generator used in this experiment is nearly identical to the one used in recent work with E85 fuel [6]. It is based on solid-state electronics and uses magnetic pulse compression to shape the output pulse. Based on current and voltage measurements across a 200 Ω resistor, it is capable of delivering a 40 kV 12 ns (FWHM) pulse with a maximum energy of 40 mJ per pulse. The voltage amplitude is scalable while maintaining the same pulse width down to an output voltage of 15 kV. If the amplitude is sufficiently low for a given gas density, only primary corona streamers are generated [13]. However, to provide effective ignition for lean conditions, higher-amplitude pulses had to be used, but still with a 12ns FWHM duration. The higher amplitude leads to breakdown of the gas and formation of a spark with a very short time duration. Since the spark gap is a more complex load than a resistor, the exact amount of energy delivered to the spark plug is not known for these engine experiments.

The pulse generator was connected to the spark plug using a standard solid-core spark-plug wire and boot. Both the spark plug wire and the boot were shielded with a custom wire-mesh sheathe that was connected to ground of both the cylinder head and the pulse generator. The pulse generator was operated in burst mode, in which 10 pulses were delivered at a repetition rate of 10 kHz. The timing for the first of the 10 pulses was controlled by custom electronics coupled to the shaft encoder of the engine. After the first pulse was triggered, the remaining 9 pulses were triggered in time domain, with the 10-pulse burst spanning 0.9 ms in total. Because of the very short pulse duration, each arc is terminated before it enters its glow phase. Therefore, the name “multi-pulse (MP) transient plasma ignition” was introduced in the recent lean-burn study [6].

Experimental Procedure and Data Analysis

For each operating point with the all-metal engine configuration, the engine is allowed to run for several minutes until all measured parameters are stable, at which point data are acquired. Fuel-flow rate and thermocouple readouts are averaged over one minute. The in-cylinder pressure, spark current for the regular inductive system, intake and exhaust pressure, and fuel pressure are acquired for 500 consecutive cycles using 0.1°CA resolution. For the in-cylinder pressure, an uncooled Kistler 6125C piezoelectric sensor is used in combination with a Kistler 5010B charge amplifier. Day-to-day repeatability is very good, with variations of average indicated mean effective pressure (IMEP) of less than 2%.

The apparent heat-release rate (AHRR) is computed from the in-cylinder pressure for each individual cycle using a constant ratio of specific heats ($\gamma = 1.33$) following [4]. For computing combustion-phasing metrics like the 50% burn point (CA50), the AHRR is integrated over the crank-angle range for which AHRR is positive. For all data presented, except for the graphs in Figs. 17 & 20, this computation of burn points is performed in a conventional way, whereby the integral of AHRR is scaled so that it rises from 0 to 100% for every cycle, irrespective of the actual η_{comb}. For the burn-point-based AHRR profiles in Figs. 17 & 20, the final burn point for each cycle varies according to an estimate of the combustion efficiency for each cycle. The latter is computed from the integral of the AHRR and the average η_{comb} derived from exhaust-emissions measurements. This refined technique allows examining on a per-cycle basis how changes to the AHRR profile affect the combustion efficiency.

To quantify $IMEP_n$ instability, the standard deviation (SD) of IMEP is first computed for all 500 cycles. As a measure of the relative

$IMEP_n$ instability, the corrected standard deviation (CSD) of IMEP is computed:

$$\text{CSD of IMEP}\,[\%] = 100 \cdot \frac{SD_{IMEP_{fired}}}{(IMEP_{fired} - IMEP_{motored})} \qquad (3)$$

This is identical to the traditionally used coefficient of variation (COV), except that the denominator has been corrected for the heat-transfer and blow-by losses of a motored cycle. The difference in IMEP for fired and motored operation equals the IMEP rise caused by the combustion event. This definition allows the relative $IMEP_n$ instability to be consistently evaluated even for operation with IMEP near zero or negative, see Ref. [14] (*e.g.* idle operation or vehicle coasting.) For operation at the moderate loads of this study, CSD values are only slightly lower than COV values. Furthermore, the value of CSD of IMEP does not depend on the definition of IMEP (*i.e.* compression-expansion for gross, or all four strokes for net), provided that the gas-exchange strokes are repeatable. (In this study, the gas-exchange strokes are very repeatable as a result of the selected constant valve timings.) In the following, CSD of $IMEP_n$ will be referred to as $IMEP_n$ instability.

Presented values of mass-averaged temperature at the time of spark are computed using the ideal-gas law in combination with the measured pressure (averaged over 500 cycles), the known cylinder volume, and the trapped mass. The trapped mass equals the sum of the supplied air, N_2, fuel, and residuals. The average molecular weight used in the ideal-gas law corresponds to the mixture of fresh charge and residuals. As such, the computed temperatures correspond to the mass-averaged temperature of a single-zone model, ignoring potential thermal stratification in the combustion chamber. To guide the understanding of end-gas autoignition, estimated end-gas reactant temperature ($T_{end\text{-}gas}$) is reported as well. It is computed using Eq. 4, with the assumption of isentropic (no heat release) and adiabatic (no heat transfer) compression by the combustion-induced pressure rise that occurs after the spark timing (ST).

$$T_{end-gas} = T_{avg@ST} \cdot \left(\frac{P_{actual}}{P_{ST}} \right)^{\left(\frac{\gamma - 0.07 - 1}{\gamma - 0.07} \right)} \qquad (4)$$

$T_{avg@ST}$ and P_{ST} correspond to the mass-averaged gas temperature and pressure at the time of spark, respectively. (Note that ST is quite early, -57 to -38°CA, for the operating points were $T_{end\text{-}gas}$ is plotted. Therefore, heat transfer does not affect $T_{avg@ST}$ substantially for those operating points.) P_{actual} refers to the pressure at any crank angle after ST. γ represents the ratio of specific heats. For each operating point, γ is determined from the measured rise of pressure and computed rise of mass-averaged gas temperature that occur between IVC and ST. The subtraction of 0.07 from γ in Eq. 4 is performed to compensate for the reduction of γ that occurs as the gas temperature keeps rising after ST. To allow estimating the accuracy of this method, Appendix A shows a comparison with a more elaborate method to compute the end-gas compression heating based on the thermodynamic library built into CHEMKIN-PRO. It should be noted that heat release due to autoignition reactions will cause the actual temperature of the end-gas reactants to be higher than $T_{end\text{-}gas}$, but a treatment of this is the beyond the scope of the current study.

Fuels

This study is focused on a comparison of gasoline and E30. It also includes one data point using E85. Table 2 provides a comparison of octane numbers.

Table 2. Measured octane numbers for gasoline. Octane numbers for E30 and E85 are estimated based on ethanol-blending trends in Ref. [15].

Fuel	**Gasoline**	**E30**	**E85**
AKI	92.7	98	100
RON	96.6	104	108
MON	88.7	91	91

The gasoline was supplied by Haltermann Solutions as an exhaust-emissions and fuel-economy certification fuel for the US market. Key properties are listed in Table 3.

Table 3. Specifications of Haltermann certification gasoline

Density [kg/l]	0.743
Carbon, wt%	86.7
Hydrogen, wt%	13.3
Oxygen, wt%	none detected
A/F Stoichiometric	14.54
Lower Heating Value, gas-phase fuel [MJ/kg]	42.57
LHV for stoichiometric charge [MJ/kg]	2.738
Hydrocarbon Type, vol%	
Aromatics	32.7
Branched Alkanes	55.0
Linear Alkanes	7.5
Cyclic Alkanes	2.9
Alkenes	0.07
Not Classified	1.9
Distillation, °C	
5%	43
10%	51
30%	75
50%	103
70%	116
90%	158
95%	171

The E30 fuel was prepared in-house by blending the Haltermann certification gasoline with anhydrous high-purity ethanol in 70%/30% proportions by volume. With the assumption of a linear variation of properties upon blending, some estimated properties of the E30 fuel are given in Table 4.

The E85 fuel was also prepared in-house, but in 15%/85% proportions by volume. However, the gasoline fuel used for the E85 blending is a Chevron-Phillips research-grade gasoline, which has a slightly lower antiknock index of 87 [6].

Table 4. Estimated properties of E30 fuel blended from the high-octane certification gasoline.

Specific gravity	0.757
A/F Stoichiometric	12.81
Lower Heating Value, gas-phase fuel (MJ/kg)	37.9
LHV for stoichiometric charge (MJ/kg)	2.747
Hydrocarbon Type, vol%	
Oxygenates	30.0
Aromatics	22.9
Branched Alkanes	38.5
Linear Alkanes	5.2
Cyclic Alkanes	2.0
Alkenes	0.05
Not Classified	1.4

Results

These tests employ swirling in-cylinder flow for consistency with a recent lean-burn study in the same engine [6]. The swirling flow is accomplished by deactivating one of the intake valves, as noted previously in conjunction with Table 1.

Table 5 shows the operating conditions that are common to all ϕ_m-sweeps that use the regular spark (RS) system. Fuel was injected during the intake stroke using three injections of equal duration to create a well-mixed charge of fuel, air, N_2 and residuals. Moderate adjustments to the injection timing between data points were performed for E30 to achieve low soot emissions while maximizing the available time for fuel-air mixing. It was found that near-stoichiometric data points for E30 required SOI = -300°CA to keep the smoke levels near zero. On the other hand, the lean-stability limits improved with an earlier SOI = -330°CA. In contrast, gasoline operation did not require such SOI adjustments to maintain low smoke, so SOI = -330°CA was used throughout. All highly lean or dilute operating points were operated with SOI = -330°CA, so the lean and dilute stability limits can be compared directly between fuels.

The selected valve timings result in low residual levels (≈4-6% by mass). For each fuel, the fuel mass per cycle was first established for stoichiometric operation without N_2 dilution. The target was to achieve a net indicated mean effective pressure ($IMEP_n$) of 370 kPa. For subsequent data points at other ϕ_m, this fuel mass was held constant. Stoichiometric operation is highly throttled due to the relatively low load, with an absolute intake pressure (P_{in}) of only 45-46 kPa. As the charged is leaned out by metering more air into the intake system, the intake pressure rises. For the leanest operating points, P_{in} reaches 93 kPa.

Effect of Combustion Phasing for Lean E30 Operation

The selection of spark timing (ST) and combustion phasing are critically important for the engine performance. This section discusses how spark-timing and combustion-phasing targets shift with changes of ϕ.

Table 5. Operating conditions for ϕ_m-sweeps with regular spark system.

Injection Pressure	170 bar	
# of Fuel Injections	3	
ΔCA between SOIs of Fuel Injections	15°CA	
Spark Energy	106 mJ	
Coolant Temperature	75°C	
IMEPn @ ϕ = 1 without dilution	370 kPa	
Fuel	**Gasoline**	**E30**
Fuel per Cycle	15.6 mg	17.8 mg
Intake Pressure @ ϕ = 1 (unheated)	46 kPa	45 kPa
Intake Pressure Range	37 - 93 kPa	45 - 89 kPa
Start of First Injection	-330°CA	-330° to -300°CA
Spark Timing Criteria	1) Avoid misfires, 2) Avoid strong audible knock, 3) CA50 = 5°CA	1) Avoid misfires, 2) Avoid strong audible knock, 3) For maximum IMEPn (MBT)

Figure 3d shows how the net indicated thermal efficiency (η_{th}) varies with CA50 for two different operating points. For the unheated stoichiometric case, highest η_{th} is encountered for CA50 ≈ 10°CA. (For consistency with common literature descriptions of spark timing for maximum brake torque, this data point is labeled MBT. It was determined by sweeping ST in small steps, but only two stoichiometric data points were acquired for Fig. 3.) In contrast, the lean heated operation with ϕ = 0.55 requires a much earlier CA50 to attain MBT phasing. For this lean operating point, there are three main contributors to the improved η_{th} with advancing combustion phasing in the CA50 = 17 – 4°CA range,:

1. Higher combustion efficiency (η_{comb}), see Fig. 3a.
2. Shorter combustion duration (Fig. 3b).
3. Better combustion phasing with less AHRR during the expansion stroke (Fig. 4), *i.e.* larger fraction of constant-volume combustion.

The higher combustion efficiency is coupled to the disappearance of partial-burn cycles that plague the $IMEP_n$ stability for lean operation with late combustion phasing, see Fig. 3c. On the other hand, Fig. 3c shows that the $IMEP_n$ instability increases rapidly for overly advanced CA50. This is caused by the appearance of complete misfire cycles. Figure 5a shows that the AHRR for operation with ST = -57°CA has substantial cycle-to-cycle variations, but the combustion proceeds without misfires.

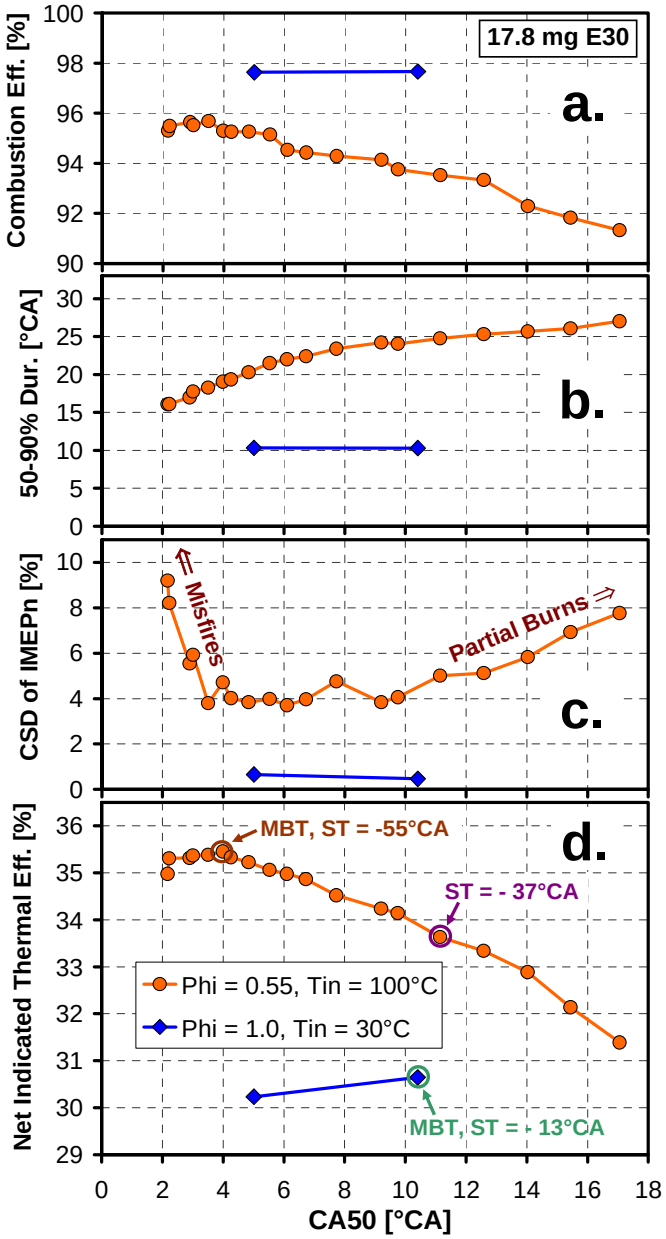

Figure 3. Effect of combustion phasing on a) combustion efficiency and b) 50-90% burn duration, c) IMEP instability, and d) thermal efficiency for both stoichiometric and lean heated operation with E30 fuel.

When ST is advanced to -65°CA, Fig. 5b shows that 2 out of 250 cycles misfire completely; see example cycle without positive AHRR plotted in blue. The misfires occur partly because of the low compressed-reactant temperature at the time of spark. Analysis of this spark-timing sweep with ϕ = 0.55 indicates that a reactant temperature of 570K is required to ensure successful inflammation for all cycles. Below this temperature, the flame speed becomes too low to ensure robust flame development for this low ϕ, as demonstrated in Ref. [6]. (For higher ϕ, robust flame development can be achieved even if the temperature is lower than 570K.) The importance of the reactant temperature at the time of spark will be discussed more in the section that compares the RS system with the MP ignition system. The exact reason for the appearance of the two misfires in Fig. 5b is not known. Examination of the spark-current waveform for these cycles reveals that the misfires are not caused by a failure to form a spark plasma, leaving turbulent fluctuations of the flow field as a potential reason [16].

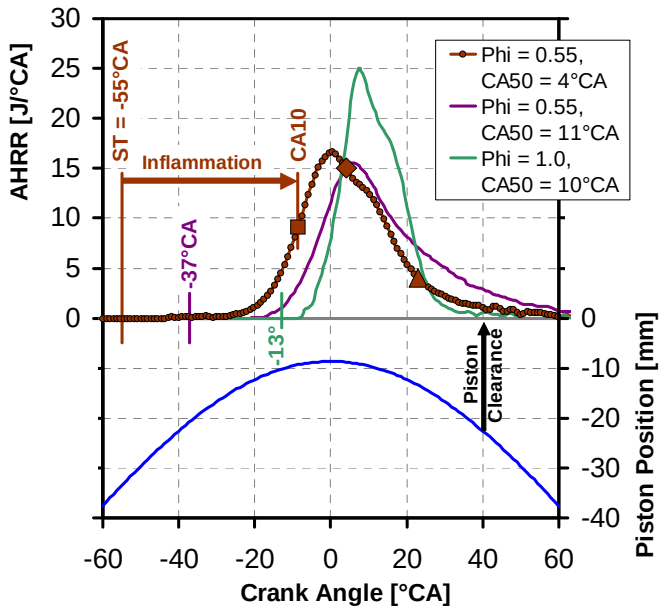

Figure 4. Combined effects of ϕ and combustion phasing on ensemble-averaged heat-release profile relative to the piston motion. (Piston clearance is here defined to be the area-averaged vertical distance between the piston top and the cylinder head.) Larger symbols on the AHRR trace for the more advanced ϕ = 0.55 operating point mark the points for CA10 (square), CA50, diamond), and CA90 (triangle).

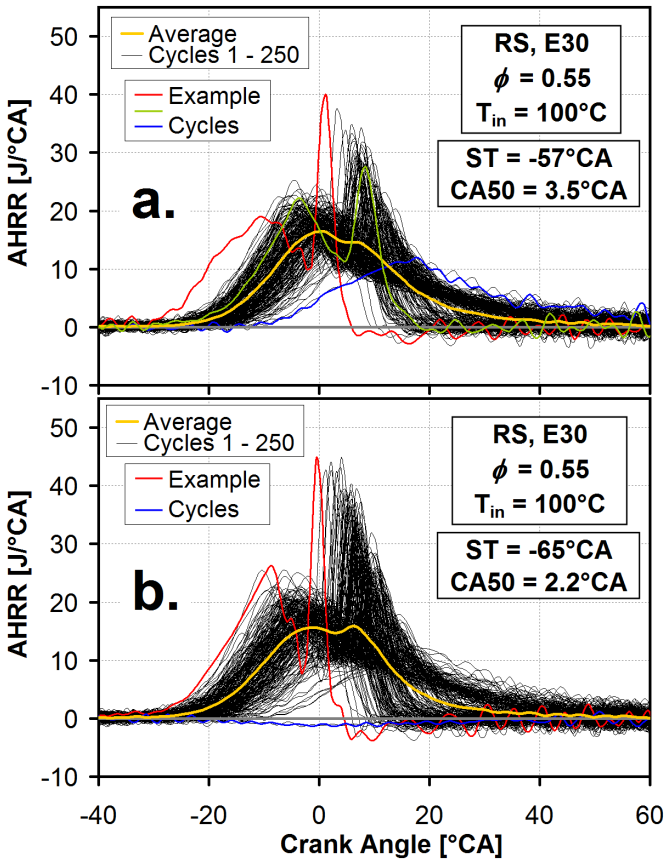

Figure 5. Onset of end-gas autoignition, but also misfires for STs earlier than that of MBT timing. Lean heated E30 operation with RS system.

Combustion Terminology

The term "successful inflammation" in the preceding paragraph refers to creating a flame kernel that survives its nascent laminar state and transitions into fully developed turbulent deflagration. The time scale for inflammation is an important factor that influences the level of cycle-to-cycle variations. It will be useful to discuss some of the following results in terms of "inflammation time". For quantitative comparisons, inflammation time is equated to the spark-to-CA10 delay, as illustrated for one of the operating points in Fig. 4. Furthermore, CA50 is equated to combustion phasing. Combustion duration and the term "main combustion phase" both refer to the CA10 – CA90 range. To provide specific examples, larger symbols represent CA50 (diamond) and CA90 (triangle) for the same operating point in Fig. 4.

Lean Mixed-mode Combustion

Figure 5 can also help to explain the 50-90% burn-duration trend in Fig. 3b. It is remarkable that the trend is steepest for the earliest CA50 data points. The example cycles plotted in red and blue in Fig. 5a are selected to have very different combustion phasings. The more advanced red cycle displays a second sharp peak indicative of end-gas autoignition. It also displays a crisp end of the combustion. Here, such combination of deflagration followed by end-gas autoignition is termed mixed-mode combustion. In contrast, the cycle plotted in blue in Fig. 5a only displays one broad peak, indicative of only deflagration-based AHRR. An examination of the two collections of AHRR profiles in Fig. 5 reveals that mixed-mode combustion becomes more frequent with an earlier average CA50. From an efficiency standpoint, the crisp end of combustion associated with end-gas autoignition this is a desirable feature of lean combustion since it has potential to ensure that all, or nearly all, chemical energy is converted to heat near TDC prior to excessive combustion-chamber expansion. The ensemble-averaged AHRR curves are plotted in yellow. They reveal that the end-gas autoignition is sufficiently repeatable to create dual-peak AHRR profiles, with a more distinct second peak for the case with the earlier ST. Re-examining Fig. 3b shows that the fast reduction of the 50-90% burn duration for earlier CA50 in the 2 – 8°CA range is consistent with the observed crisper end of combustion for early-phased cycles that display end-gas autoignition.

The mixed-mode combustion studied here has similarities to spark-assisted compression ignition (SACI), which also features a combination of flame and end-gas autoignition [17]. One drawback of mixed-mode combustion is the risk of producing excessive and erratic noise. Figure 5a shows that there are large cycle-to-cycle variations of the deflagration-based AHRR in the -30°CA to TDC range. These variations cause strong variations of the end-gas autoignition-based AHRR, both in terms of timing and magnitude of the corresponding peak. Cycles with strong early deflagration lead to an earlier onset of end-gas autoignition, and the associated peak AHRR is greater. For a typical cycle, this causes a mild pressure oscillation. To illustrate this, Fig. 6 plots the raw and filtered pressure traces corresponding to the two specific examples of AHRR traces with end-gas autoignition in Fig. 5a. The pressure trace for the strongest red example cycle displays a peak-to-peak magnitude of roughly 0.4 bar shortly after the onset of end-gas autoignition at -2°CA. The green example cycle also has a peak AHRR that is stronger than the statistical average. Figure 6 shows that its pressure ripples are very weak. This is consistent with the sound experience during data acquisition. Audible knock is only heard for outlier cycles with early and strong end-gas autoignition. The typical cycle generates audible noise that is only marginally harsher than standard SI combustion cycles without end-gas autoignition. However, further work is needed to quantify the noise level.

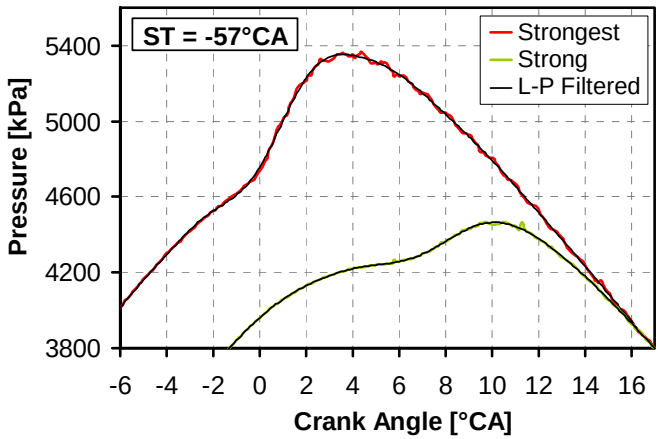

Figure 6. Illustration of weak ripples of the pressure traces corresponding to the two specific examples of AHRR traces with end-gas autoignition in Fig. 5a.

For automotive applications with stringent NHV targets, the engine noise characteristics may be unacceptable for operating points that exhibit cycle-to-cycle variations of the AHRR that are comparable to those shown in Fig. 5a. In the following, the benefits of mixed-mode combustion will be quantified, while steps are taken to reduce cycle-to-cycle variations. Turbulent deflagration can generate very repeatable AHRR, as illustrated for stoichiometric operation in Fig. 7. As has been shown in Ref. [6], the key to stable deflagration-based AHRR is having a short induction time from spark to the main combustion phase. Short induction time is inherent to near-stoichiometric operation due to the quickly developing flame kernel, but can be challenging to achieve for lean or dilute operation due to lower flame speeds.

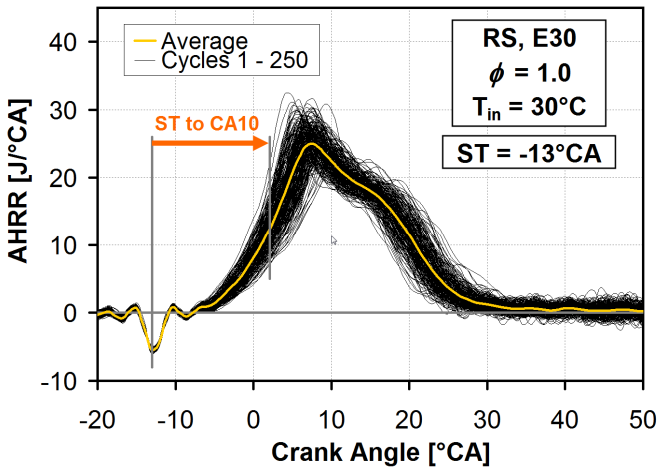

Figure 7. Illustration of high combustion stability for stoichiometric E30 operation with RS system.

Comparing Lean and Dilute Operation with Gasoline, E30 & E85 Using Regular Spark System

Lean or dilute operation can improve the thermal efficiency. This section summarizes the results from four ϕ- or ϕ_m- sweeps with either fuel, as listed in Table 6. The operating conditions of these sweeps also correspond to Table 5. For each fuel, there are two lean ϕ- sweeps where air is used as the oxidizer ($[O_2]$ = 20.9%), and two stoichiometric dilute ϕ_m - sweeps where $[O_2]$ is reduced by the addition of N_2. For each type, two different intake temperatures are used.

Table 6. Data sets with ϕ- or ϕ_m- sweeps for gasoline and E30 with regular spark system.

Data set	Intake Air Temperature	ϕ	ϕ_m	Intake O_2 Mole Fraction
Lean	30°C	0.54 - 1.3	⇐	20.9%
Heated Lean	100°C	0.50 - 1.0	⇐	20.9%
Dilute	30°C	1.0	0.62 - 1.0	11.8 - 20.9%
Heated Dilute	100°C	1.0	0.57 - 1.0	11.8 - 20.9%

In total, eight data sets are presented for gasoline and E30, using the regular spark system. Selected metrics are plotted in Figs. 8 & 9. The bottom row of Table 5 lists the criteria used to set ST, in order of priority. For E30, MBT timing was targeted. However, for gasoline, the targeted combustion phasing, measured as CA50, was 5°CA aTDC. This combustion phasing was chosen for consistency with the E85 data published in Ref. [6]. On the other hand, the heated near-stoichiometric gasoline data points had to be operated with CA50 > 5°CA to avoid onset of excessive audible knock. As a result, the CA50 trends for heated lean operation are comparable for the two fuels. For ϕ = 1, the two fuels have identical CA50 values and for ϕ near peak η_{th}, gasoline is only slightly less advanced. These heated lean data sets also provide the largest gains of η_{th} relative to stoichiometric, non-diluted $\phi = \phi_m = 1$ operation.

To avoid confusion about the unit for changes of η_{th} relative to that of ϕ_m = 1 operation (*i.e.*, absolute %units vs. relative % change), the term fuel economy (FE) is used for these discussions despite only one combination of engine speed and fueling rate being examined. Figure 9a shows that FE of heated lean gasoline operation increases by roughly 20% for ϕ = 0.52 - 0.55. In contrast, the largest FE improvement is only 17% for E30, shown in Fig. 8a. This difference can be attributed to the higher octane numbers of E30, which make it harder to achieve mixed-mode combustion for this operating point. This is illustrated in Fig. 10, which plots ensemble-averaged AHRR traces for gasoline, E30, and also E85 operated lean with heated intake and ϕ = 0.55.

Figure 10 shows that the three fuels have nearly identical deflagration-based AHRR until TDC, at which point the AHRR of gasoline deviates due to the onset of end-gas autoignition. As a result, the AHRR of gasoline keeps rising until a peak has been reached at 10°CA, and falls off rapidly thereafter. Due to this change of the AHRR profile, more heat is released earlier in the expansion stroke, yielding a larger gain of η_{th}. Both E30 and E85 display a slow burn-

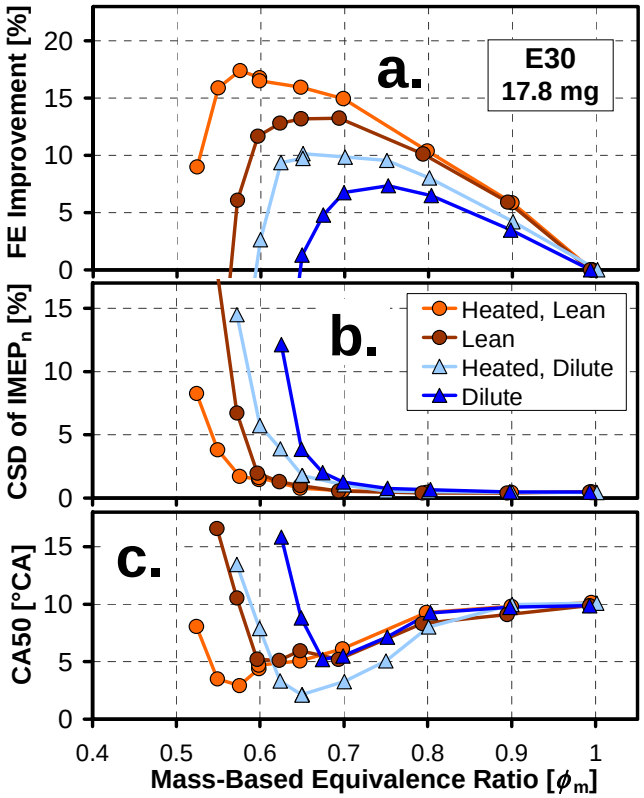

Figure 8. E30 fuel with RS system. a) Improvement of fuel economy relative ϕ = 1. b) $IMEP_n$ variability, and c) combustion phasing.

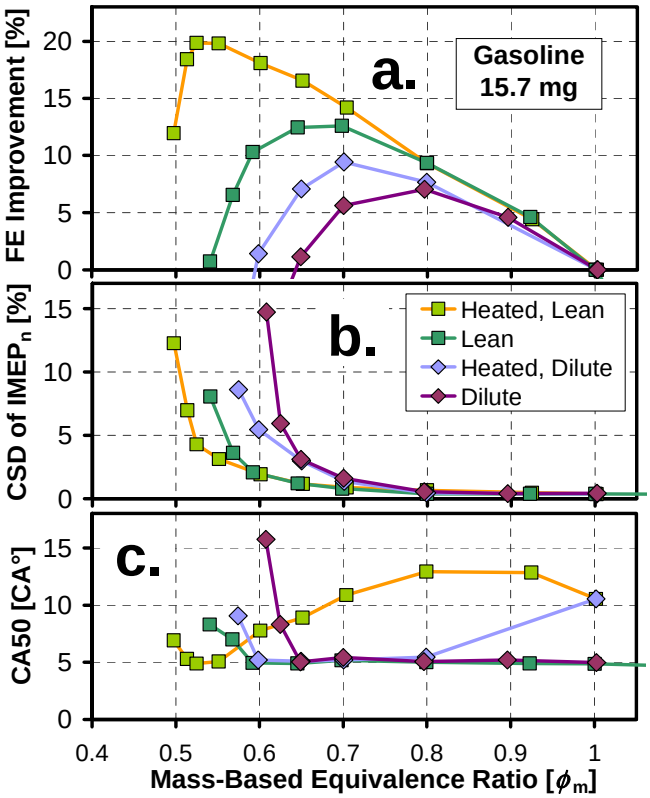

Figure 9. Gasoline with RS system. a) Improvement of fuel economy relative ϕ = 1. b) $IMEP_n$ variability, and c) combustion phasing.

out process with substantial heat being released after 20°CA, at which point the piston has descended substantially (cf. Fig. 4). Consistent with their very similar AHRR profiles, the heated lean ϕ -sweep of E85 in Ref. [6] also displays a maximum FE gain of 17%. Since the fuel was injected directly into the cylinder, it should be noted that the stronger vaporization cooling of E30 and E85 may contribute to the lack of end-gas autoignition for these operating conditions [18].

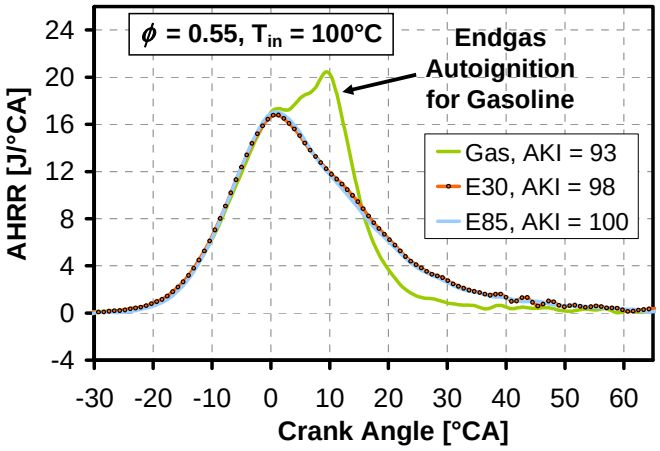

Figure 10. Comparison of ensemble-averaged AHRR for heated lean operation with gasoline, E30 and E85.

This observed benefit of a shorter burn duration is consistent with a lean-burn study by Ayala *et al*. [19]. They found that at the ϕ where the 10-90% burn duration equals 30°CA, no additional gain of thermal efficiency will be realized if ϕ is further reduced. For the operating points presented in Fig. 10, gasoline has an average 10-90% burn duration of 23°CA, whereas it is approximately 32°CA for both E30 and E85.

Compared to heated lean operation, Figs. 8 & 9 show that the other modes of operation provide less η_{th} benefit for either fuel. As summarized in Fig. 11, non-heated lean operation is inferior to heated lean operation. The main reason for this difference is the much faster development of the flame kernel associated with heated intake operation [6]. Stoichiometric dilute operation offers the smallest η_{th} benefit for either fuel, with roughly 10% FE gain for heated dilute and 7% for non-heated dilute.

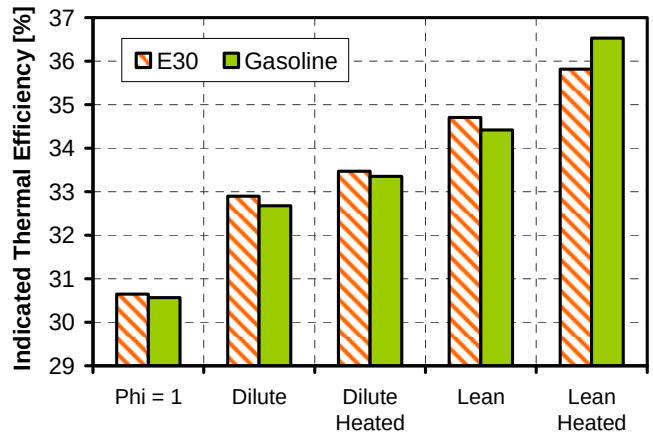

Figure 11. Summary of peak thermal efficiency corresponding to ϕ_m of data points with largest TE improvement in Figs. 8a & 9a.

The relatively low FE benefit of dilute operation is largely explained by the associated slow early flame development and slower overall heat release. Figure 12 compares dilute and lean operation without intake heat at ϕ_m = 0.70, for both gasoline and E30. First, the AHRR profiles are nearly identical for the two fuels at these two operating conditions. This illustrates that the differences in octane numbers have no effect for these operating points without intake heat, in strong contrast to the results for heated lean operation shown in Fig. 10. Second, Fig. 12 shows that the dilute operation has an AHRR profile that is broader, which means a reduction of both the degree of constant-volume combustion and the work-extraction efficiency.

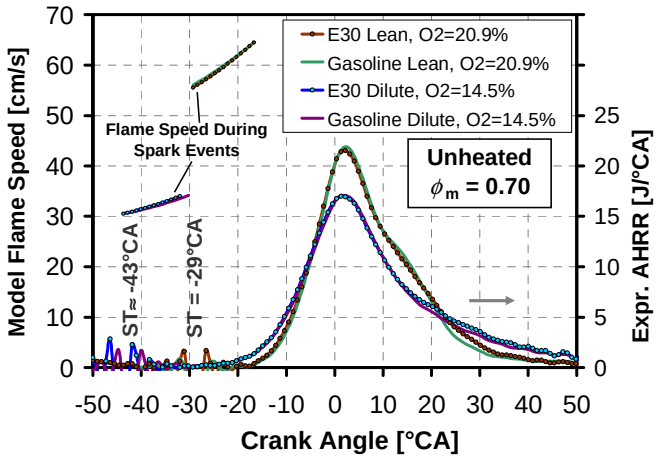

Figure 12. Comparison heat-release rate for unheated dilute operation with gasoline and E30. Laminar flame speeds are shown for CAs during spark discharge. These were predicted using a detailed chemical-kinetics mechanism where E30 and gasoline were represented by 5- and 4-component surrogate mixtures, respectively [20].

Not evident in Fig. 12 is a reduction of η_{comb} by roughly 2.5% for dilute operation at ϕ_m = 0.70, relative to that of lean operation at ϕ = 0.70. Based on differences in measured CO emissions for lean and dilute operation it is estimated that almost half of this η_{comb} reduction is caused by an inability of stoichiometric combustion to fully complete due to dissociation of CO_2 in the hot O_2-depleted gases [3,4]. This is a fundamental barrier that prevents even the best optimized dilute operation to reach as high thermal efficiency as lean operation. Nonetheless, due to the availability of cost-effective NO_x aftertreatment with a conventional three-way catalyst for stoichiometric operation, there is strong motivation to enhance dilute operation.

In addition to the slow main combustion phase, Fig. 12 reveals another challenge with dilute stoichiometric operation, namely the need to advance the spark timing strongly to maintain combustion phasing. In the examples of Fig. 12, ST has to been advanced from -29°CA to -43°CA. This is necessary due to much slower inflammation. CHEMKIN-PRO modeling results that correspond to the in-cylinder conditions for the duration of the spark discharge are plotted against the left-hand axis of Fig. 12 [20]. They reveal a strong reduction (≈ -45%) of the laminar flame speed during the spark-discharge period[1]. This is a combined effect of the reduction of [O_2]

[1] Analysis of the spark-current data shows that the average spark duration is roughly 13°CA. The duration is indicated by the span of the flame-speed results for each condition in Fig. 12.

and the lower reactant temperatures for the earlier ST of the dilute cases.

The difference in required ST for lean and dilute operation increases with a further reduction of ϕ_m, as illustrated for gasoline in Fig. 13b. The largest ST difference is found for ϕ_m = 0.65. For more dilute operation, ST has to be retarded to avoid misfire cycles, similar to that of lean operation discussed in conjunction with Fig. 5. As a result, the target CA = 5°CA can no longer be maintained, see Fig. 13b.

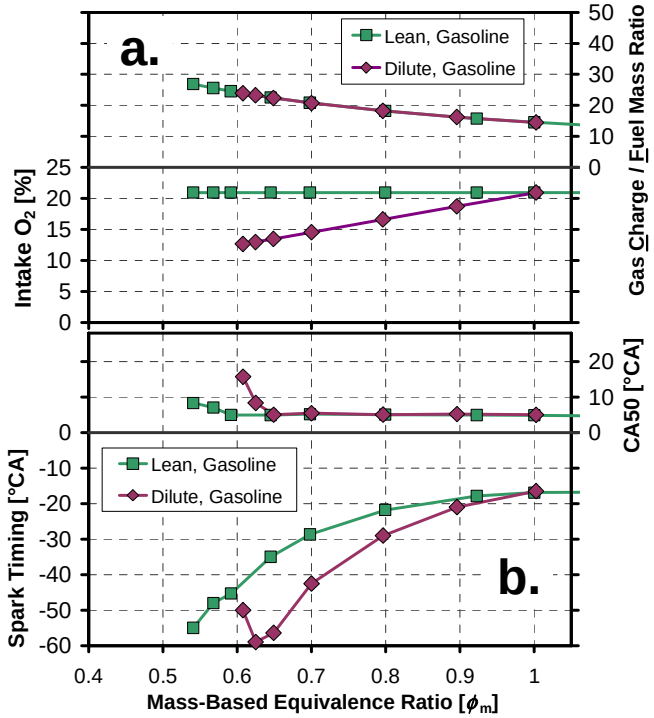

Figure 13 a) Variation of C/F ratio and [O_2] with ϕ_m for lean and dilute gasoline operation without intake heat. b) ST used to attain target CA50 = 5°CA.

Figure 13a plots the reduction of intake [O_2] for dilute operation. To demonstrate the practical use of ϕ_m, the ratio of intake charge mass to fuel mass (C/F) is plotted on the right-hand axis in Fig. 13a. The lean and dilute data points collapse to one line. This demonstrates that the use of ϕ_m effectively plots data points for both lean and dilute operation against the effective mass-dilution level, consistent with the definition of ϕ_m in Eq. 1.

The need to use a much earlier ST to maintain combustion phasing for dilute operation ultimately limits the attainable mass-dilution level. Figures 8b & 9b show that the onset of $IMEP_n$ instability occurs at substantially higher ϕ_m for dilute operation, regardless of fuel or intake temperature. For each data set in Figs. 8 & 9, the inability to maintain target CA50 at the lean and dilute limits is correlated with the rapid increase of $IMEP_n$ instability as plotted in Figs. 8b & 9b. This happens due to the overriding criterion of avoiding misfire cycles, as listed in the bottom row of Table 5. Near the lean and dilute limits, ST therefore needs to be retarded so that the spark ignition takes place in reactants that are compressed to higher temperatures.

To summarize, both lean and dilute operation offer substantial improvements of η_{th}, but the data also reveal that there are challenges, in particular for stoichiometric dilute operation. To achieve large improvements of η_{th}, it is important to maintain both low cycle-to-cycle variability of the combustion and short combustion duration. Dilute operation suffers from both higher combustion variability due to slow inflammation, and from longer combustion duration. The lean results with gasoline reveal that the induction of end-gas autoignition can strongly shorten the combustion duration and provide larger improvements of η_{th}. However, due to the slow inflammation from spark to the main combustion event for very lean operation, cycle-to-cycle variations of the end-gas autoignition causes concerns regarding the generation of erratic audible noise.

With this background, there are several reasons for an investigation of the use of a more powerful ignition system for lean and dilute operation. This will be examined in the following sections.

Improved Combustion Control with MP Ignition

Ultimately, lean and dilute SI operation both become limited by excessive cycle-to-cycle variations of $IMEP_n$, as exemplified in Figs. 8b & 9b. The cause of these $IMEP_n$ fluctuations can largely be attributed to cycle-to-cycle variations of the fragile early flame kernel. Using E85 fuel, high-speed flame imaging has revealed that the 10-pulse transient plasma ignition system shortens the induction time between ignition and fully developed turbulent combustion [6]. The use of MP ignition for operation with E30 fuel renders very similar results, as demonstrated by the AHRR plot in Fig. 14.

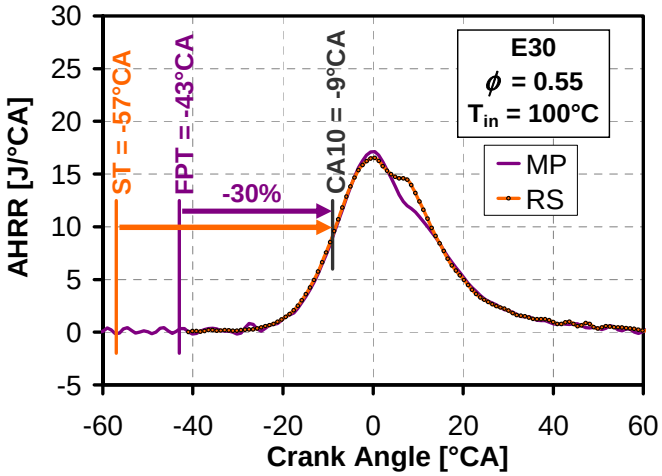

Figure 14. Reduction of spark-to-CA10 inflammation time using MP ignition for heated lean E30 operation.

Figure 14 shows that the inflammation time from spark to CA10 is reduced by 30% for the MP ignition system. (The acronym FPT in Fig. 14 refers to first pulse timing, which is equivalent to ST). The detailed physics and chemistry responsible for the faster transition to fully turbulent combustion are largely unknown, and subject to ongoing research [13,21]. Here, the MP ignition system is used to probe the potential of ultra-lean or dilute operation beyond what is possible with the current high-energy inductive spark system. As will be demonstrated, the MP ignition system does not completely resolve any of the issues encountered with the RS system. Nevertheless, it enables mixed-mode combustion for a high-octane fuel like E30, even for dilute operation. For achieving stable ultra-lean operation, it is paramount to maintain effective combustion-phasing control. For

the purpose of this discussion, the control authority is defined by Eq. 5.

$$\text{Control authority} = \frac{\Delta CA10}{\Delta ST} \quad (5)$$

Figure 15b shows that the RS system has excellent control authority for stoichiometric operation. The two data points show a 1:1 relationship between ST and CA10. This is consistent with the very short spark-to-CA10 inflammation time demonstrated in Fig. 7. In strong contrast, for lean RS operation with ϕ = 0.55 the CA10 trend is much flatter. Highest IMEP is achieved for CA10 = -9°CA, which is indicated by a dashed horizontal line in Fig. 15b. A linear fit to the data points near CA10 = -9°CA reveals a slope of only 0.25. This means that the reduction of ϕ from 1.0 to 0.55 has caused the regular spark system to lose 75% of its control authority.

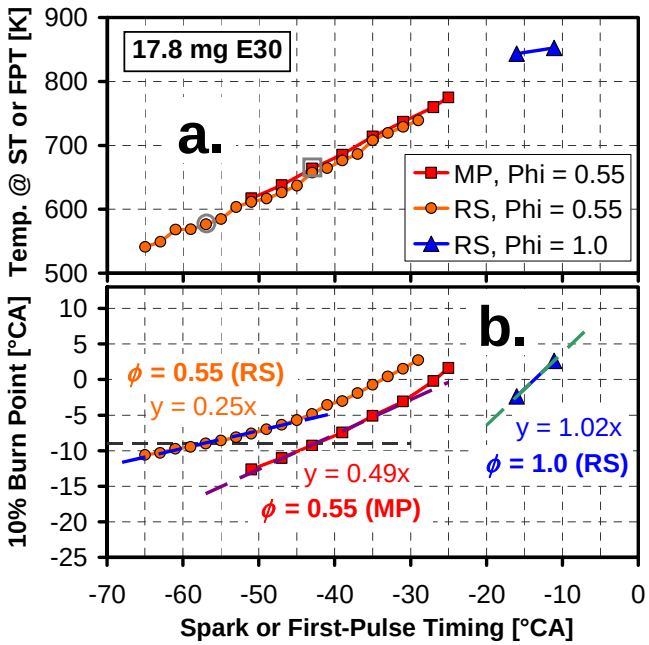

Figure 15 a) Mass-averaged temperature at CA corresponding to ST or FPT, b) control authority of ST or FPT over CA10.

The use of the MP ignition system restores a part of the lost control authority, and a linear fit to the data points near CA10 = -9°CA reveals a slope of 0.49. Hence, at this operating point with ϕ = 0.55, the MP ignition system effectively doubles the control authority. This is consistent with the 30% shorter spark-to-CA10 induction time shown in Fig. 14. Although the detailed physics of MP ignition is unknown, analysis of the data reveals that the faster inflammation for a given fixed CA10 should be partly attributed to the higher reactant temperature at the time of spark. The highlighted data points in Fig. 15a correspond to CA10 = -9°CA and show that the reactant temperature at the time of spark is roughly 87K higher for MP ignition. This is an effect of the ability to spark later with the MP ignition system while maintaining a given combustion phasing. The higher temperature at the time of spark contributes to enhance the benefits of MP ignition that stem from its specific pulse characteristics and spark-plug geometry.

Use of MP Ignition for Lean Mixed-mode Combustion

Tables 5 and 6 also apply to the operating points acquired with the MP ignition system, except that the target of CA50 = 5°CA was abandoned for gasoline. Recall that Figs. 8a & 9a show that gasoline provides higher FE gains for lean heated operation than E30 does. This can be explained by the inability of the RS system to induce repeatable end-gas autoignition of E30 for these operating points. As discussed in conjunction with Fig. 10, the mixed-mode combustion observed with gasoline provides a beneficial crisp end of the combustion event, which increases the fraction of constant-volume combustion.

With a stronger control authority, the MP ignition system can advance the combustion phasing more while maintaining high combustion stability. This can be used to induce mixed-mode combustion even for E30, as illustrated in Fig. 16. For both fuels, the end-gas autoignition is sufficiently repeatable that the ensemble-averaged AHRR profiles show distinct second peaks. The AHRR profiles are fairly similar, although E30 has a more pronounced separation of the two AHRR peaks. E30 also requires a more advanced combustion phasing. This is consistent with its higher octane numbers, see Table 2. The estimated $T_{end\text{-}gas}$ traces in Fig. 16a suggest that E30 requires 40K higher temperature for autoignition to occur. For this discussion, the onset of autoignition is defined to occur at the minimum point between the two AHRR peaks. These crank angles are marked with circles in both Figs. 16a & b, and also in some of the following figures.

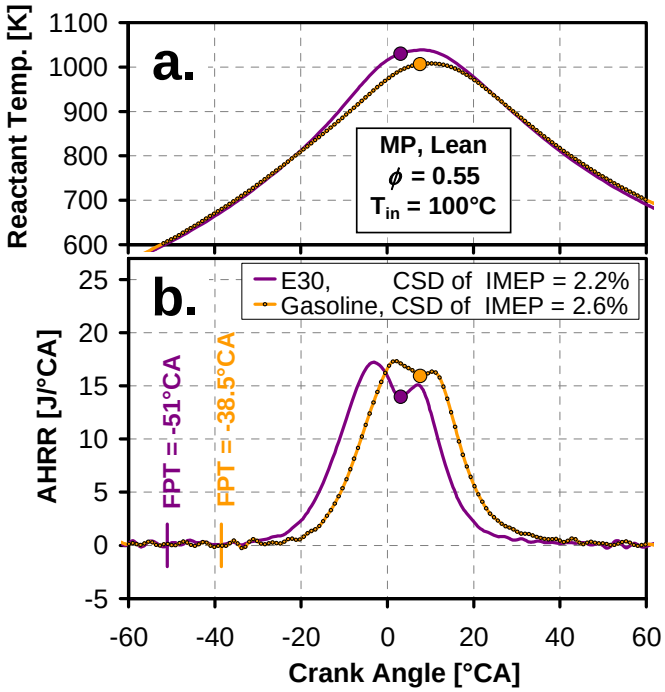

Figure 16. The use of MP ignition to induce stable lean mixed-mode combustion for both E30 and gasoline. a) estimated $T_{end\text{-}gas}$, b) AHRR.

When the MP ignition system is used to enable mixed-mode combustion of E30 at this ϕ of 0.55, it reduces CSD of $IMEP_n$ from 3.8% to 2.2% while raising the FE gain from 16% to 17%. However, E30 still falls behind gasoline in terms of efficiency, despite both fuels being operated with MBT timing in Fig. 16. A likely cause of E30's lower efficiency is its high octane number, which mandates a combustion phasing that is too advanced from a thermal-efficiency

standpoint. For operating points outside the current test matrix that would allow later mixed-mode combustion phasing (*e.g.*, higher intake temperatures), it is possible that E30 could achieve thermal efficiency comparable to gasoline.

The potential benefits of mixed-mode combustion justify further examination of the data. For better understanding of the coupling between deflagration-based AHRR and end-gas compression which leads to autoignition, the combustion process needs to be studied on an individual-cycle basis. However, the interpretation of graphs like the ones presented in Fig. 5 is confounded by cycle-to-cycle variations of the combustion phasing. To overcome this, each AHRR trace can be plotted against its own mass fraction burned (burn point). This is done in Fig. 17.

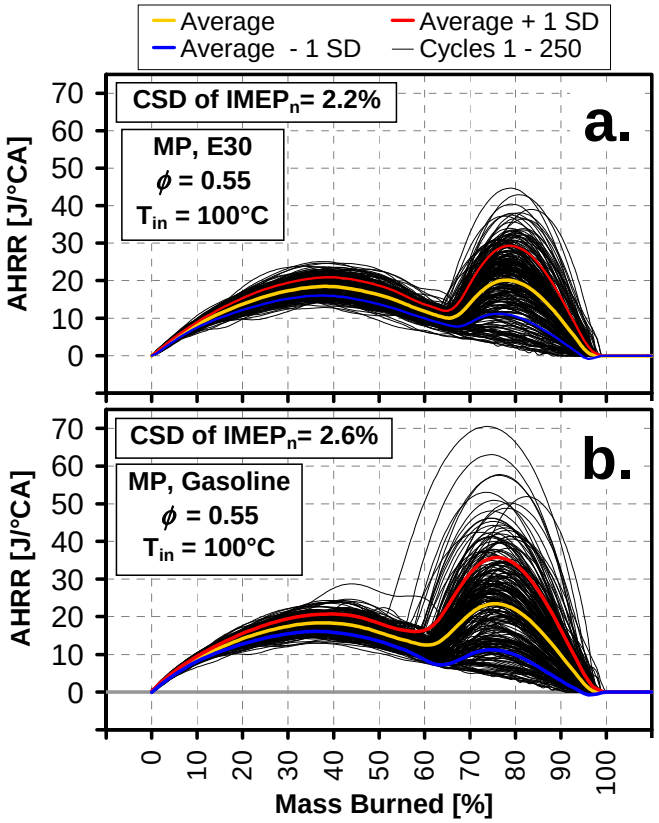

Figure 17. Comparison of mixed-mode combustion progress for lean operation with E30 and gasoline.

With the removal of combustion-phasing variability, it is easier to examine the mixed-mode combustion. The yellow line represents the statistical average for each mass fraction burned. The red and blue lines represent one standard deviation on either side of the statistical average. Figure 17a shows that for E30, the transition from deflagration to autoignition occurs on average when 65% of the available heat has been released. For gasoline, this transition occurs earlier around 62%, but it is not clear if this difference is a direct fuel effect or an effect of the earlier combustion phasing required by E30.

A comparison of the two fuels in Fig. 17 reveals that the autoignition-dominated AHRR is more intense for gasoline, with a statistical peak-average value of 24 J/°CA, vs. 20 J/°CA for E30. The stronger autoignition AHRR for gasoline is directionally consistent with a larger fraction of the fuel energy being released in an autoignition-controlled combustion process.

Furthermore, the statistical variations of the deflagration-based AHRR appear modest when each AHRR-curve is plotted against its own mass fraction burned. In contrast, the autoignition-dominated AHRR shows large cycle-to-cycle variations. Cycles that have an early transition to autoignition tends to display higher peak AHRR during the autoignition-dominated combustion phase. This is consistent with the fact that more unburned charge remains available for fast consumption by the autoignition reactions. These strong cycles also terminate the combustion process rapidly. Conversely, cycles that have a late transition to autoignition tend to display low peak AHRR. At the extreme end of the spectrum are slow-burning cycles that do not display a second AHRR peak (26 out of 250 cycles for E30). Towards the end of the combustion event, the AHRR of these cycles gradually approach zero, and for E30 8 out of 26 cycles show a final mass fraction burned in the range of 88 – 92%. This is lower than the average η_{comb} = 95.5%, which is computed from the exhaust emissions of HC and CO. These observations suggest that slow-burning cycles without end-gas autoignition contribute to a disproportional degree to the emissions of unburned HC and CO.

Use of MP Ignition for Dilute Mixed-mode Combustion

As discussed above, dilute stoichiometric operation offers less η_{th} gain compared to lean operation. This is attributed to both unfavorably long combustion duration and slow inflammation. The slow inflammation requires the use of early ST and contributes to low dilution tolerance and elevated IMEP$_n$ instability. The fact that MP ignition speeds up the inflammation for lean operation is a motivation to examine its use also for dilute stoichiometric operation. Figure 18 illustrates that MP ignition shortens the inflammation time substantially for dilute operation. At this operating point with heated intake and ϕ_m = 0.65, the regular spark system requires ST = -55°CA for MBT phasing with CA50 = 2.1°CA. Using the MP ignition system, the same combustion phasing requires FPT = -40°CA. This constitutes a reduction of the spark-to-CA10 inflammation time of 32%, which is comparable to that of lean operation shown in Fig. 14.

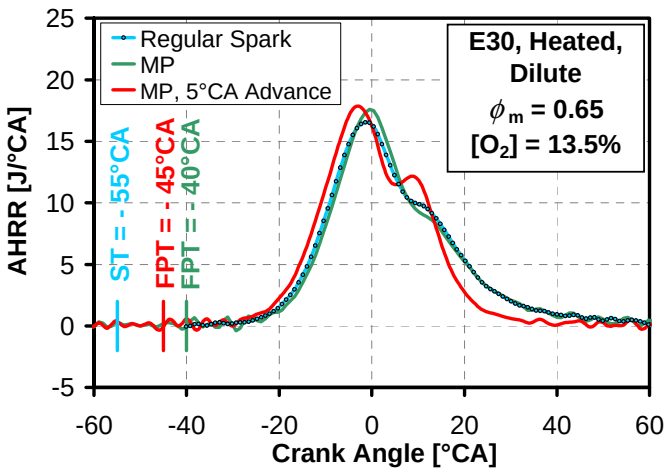

Figure 18. Comparison of RS and MP ignition systems for dilute combustion of E30.

With a faster FTP-to-CA10 inflammation, the MP ignition system offers good combustion-phasing control, with control authority = 0.57 (cf. Eq. 5, data not shown here). This can be used to advance the combustion phasing further to induce mixed-mode combustion. Figure 18 demonstrates the change of the AHRR profile that occurs

when FTP is advanced to -45°CA. With CA50 = -0.40°CA, the ensemble-averaged AHRR develops a distinct second peak around 10°CA and a crisper end of combustion.

Heated dilute gasoline operation responds similarly to the use of MP ignition. Figure 19b shows that gasoline and E30 have nearly identical AHRR profiles when CA50 is advanced to near TDC. Furthermore, Fig. 19a indicates that the end-gas autoignition temperatures are practically identical for the two fuels at this operating condition. This is remarkable given the higher octane numbers of E30. Table 2 indicates a research octane number (RON) that is 7-8 units higher for E30, and a motor octane number (MON) that is 2 units higher. At the operating conditions of Fig. 19, the effective octane index (OI) [22] must be identical for the two fuels. This implies that this particular operating point is "beyond MON". Since the gasoline and E30 have different RON-MON sensitivities, the OIs of the two fuels can assume identical values for operation that renders K > 1 [23]. Related to this, naturally aspirated HCCI experiments with heated intake have demonstrated identical autoignition reactivity for gasoline and ethanol [24], and for gasoline and E20 [25], despite large differences in octane numbers.

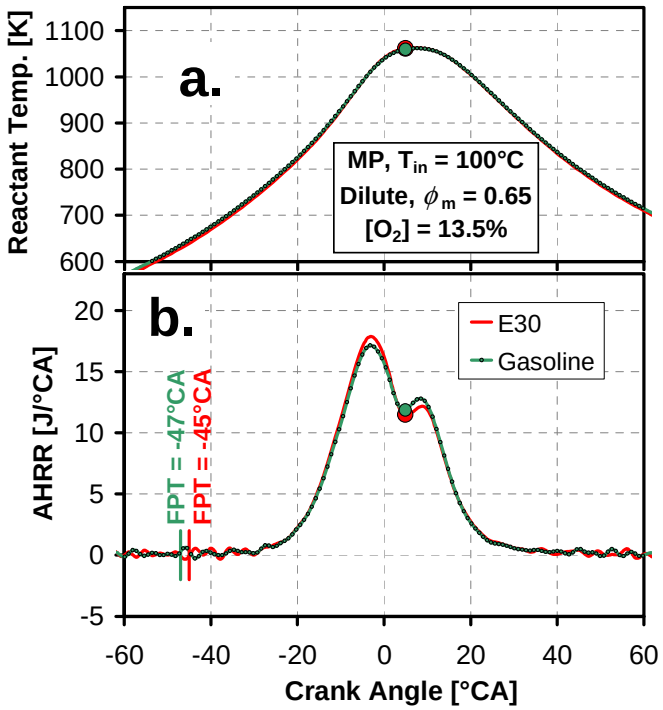

Figure 19. a) Estimated $T_{end\text{-}gas}$ and b) ensemble-averaged AHRR for MP ignition system with stoichiometric dilute operation using both E30 and gasoline.

To provide further insight into the combustion progress, Fig. 20 shows individual-cycle AHRR plotted against its individual mass fraction burned for 250 cycles. A comparison of E30 (in Fig. 20a) and gasoline (in Fig. 20b) shows that the two fuels burn very similarly. For both fuels, the transition to end-gas autoignition occurs roughly at a mass fraction burned of 68%. Compared to lean operation in Fig. 17, the dilute mixed-mode combustion has lower peak AHRR of the autoignition-dominated combustion phase, and less cycle-to-cycle variations. Still, Fig. 20 shows that both fuels exhibit some weak cycles without a discernable second AHRR peak. Even so, the final mass fraction burned is high for all but a few of the 250 cycles plotted for each fuel. The average η_{comb} is 95.5%, as computed from the exhaust emissions of HC and CO.

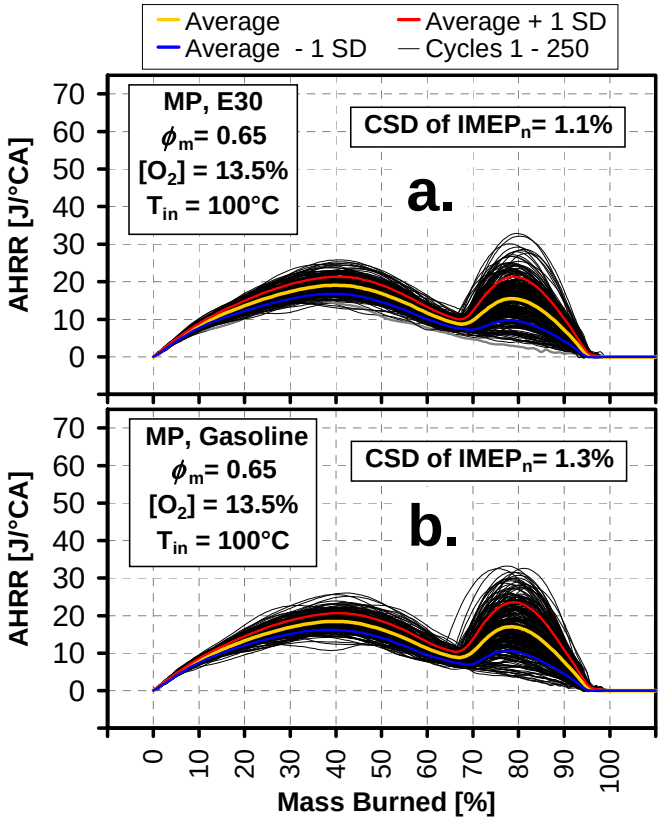

Figure 20. Comparison of mixed-mode combustion progress for stoichiometric dilute operation with E30 and gasoline.

These operating points are stable, with CSD of $IMEP_n$ = 1.1% for E30, despite substantial variations of the end-gas autoignition. Cycle-to-cycle variations of $IMEP_n$ are illustrated in Fig. 21, which includes a comparison with the corresponding baseline ϕ_m = 1.0 operating point.

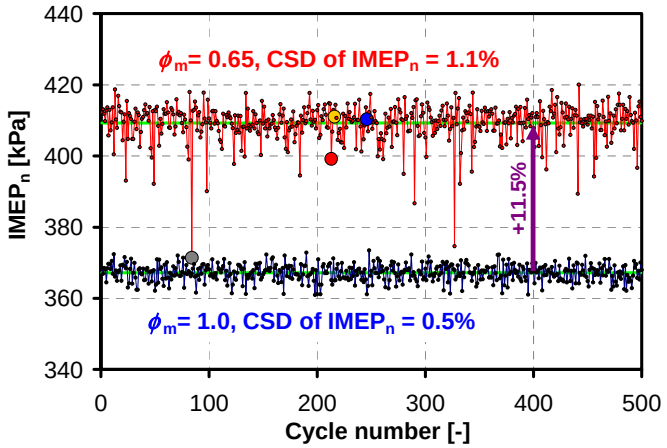

Figure 21. $IMEP_n$ variability for E30 with MP ignition, comparing heated dilute operation against stoichiometric operation.

The y-axis scale in Fig. 21 is magnified to allow a detailed examination of $IMEP_n$ variations. Most cycles are tightly clustered near the average $IMEP_n$ level, which is represented by a light-green

horizontal line for each operating point. However, the dilute operation displays numerous cycles with undesirable low $IMEP_n$. To understand if and how these $IMEP_n$ variations are linked to variations of the end-gas autoignition, four cycles are examined in detail. Cycle 84 was selected because it has the lowest $IMEP_n$ in this 500-cycle sample. It also has the weakest late-burn AHRR among the 250 cycles plotted in Fig. 20a, where it is plotted with a grey line. This cycle is also marked with a larger grey data point in Fig. 21. The other three cycles were selected to be statistically representative of having strong, typical, and weak end-gas autoignition. These cycles closely follow the burn profiles corresponding to the average, +1SD, and -1SD AHRR traces in Fig. 20a, and are using the same color scheme.

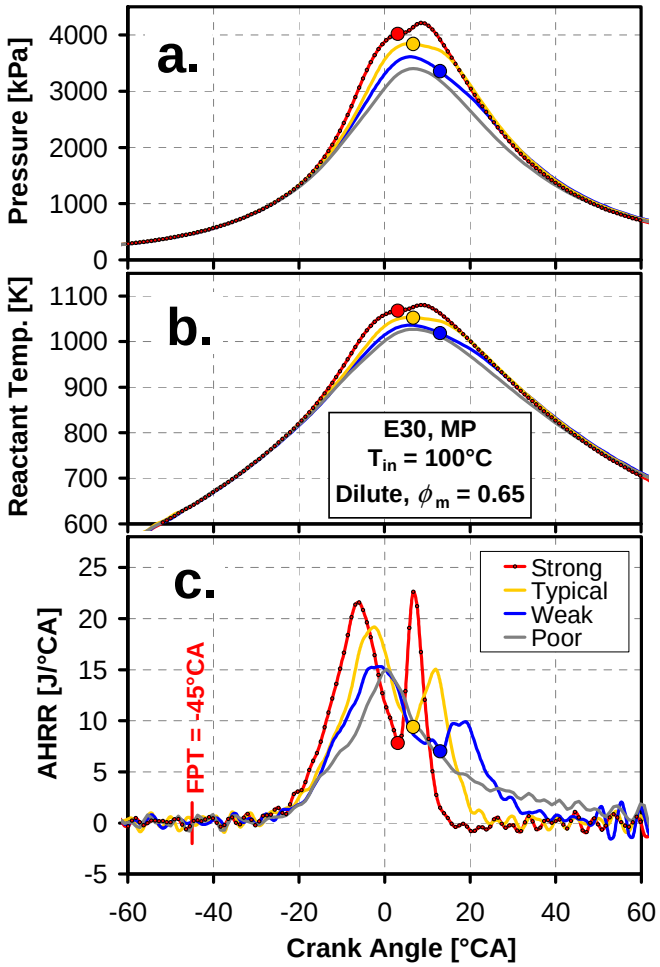

Figure 22. Demonstration of cycle-to-cycle variations of a) pressure, b) estimated $T_{end\text{-}gas}$, and c) AHRR. Dilute stoichiometric E30 operation corresponding to MP ignition case with FTP = -45°CA in Figs. 18 & 20a.

The four selected AHRR curves are plotted in CA domain in Fig. 22c. Comparing Figs. 21 and 22c, the cycles with typical and weak end-gas autoignition have near-average $IMEP_n$ values. On the other hand, the cycle with a stronger-than-average second AHRR peak has an $IMEP_n$ value that is substantially lower than the average $IMEP_n$. This can be explained by a combination of a combustion phasing that is unfavorably advanced and enhanced heat transfer caused partly by the comparably high peak AHRR [26]. Conversely, the poor-$IMEP_n$ cycle has no discernable autoignition AHRR peak. Instead its AHRR drags out and a substantial portion of the heat is released unfavorably late in the cycle, explaining its low $IMEP_n$.

Within the accuracy of the heat-release analysis, Fig. 20a indicates that its final burn fraction is near the average for this operating point, suggesting that end-gas autoignition is not required for complete combustion at this operating point. This may be a result of the comparatively advanced combustion phasing that provides sufficient time even for slow deflagration to complete before expansion cooling prevents further combustion.

These observations can guide further work towards raising η_{th} gains with the use of mixed-mode SI combustion. Figure 22b shows that the peak $T_{end\text{-}gas}$ for the typical cycle is 1053K and for the weak cycle 1036K. Hence, to achieve end-gas autoignition with an appropriately strong end-gas AHRR, $T_{end\text{-}gas}$ must be tightly controlled. This means that the stability of the deflagration-based AHRR must be further improved, both in terms of magnitude and combustion phasing. Figure 22a indicates that the deflagration-based combustion must produce a peak pressure that is stable within ±3%. Such stabilized mixed-mode operation has the potential to improve the FE gains beyond the 11.5% demonstrated in Fig. 21. From an efficiency standpoint, it would also be desirable to realize stable mixed-mode operation with a later combustion phasing.

NO_x Emissions for Heated E30 Operation

For lean SI operation, the cost and complexity of NO_x aftertreatment can be a barrier for automotive implementation [27]. Therefore, engine-out NO_x emissions are an important metric. Figure 23 exemplifies two NO_x-trends from the available data sets. Shown is a comparison of the fuel-specific NO_x for lean and dilute heated RS operation with E30 fuel.

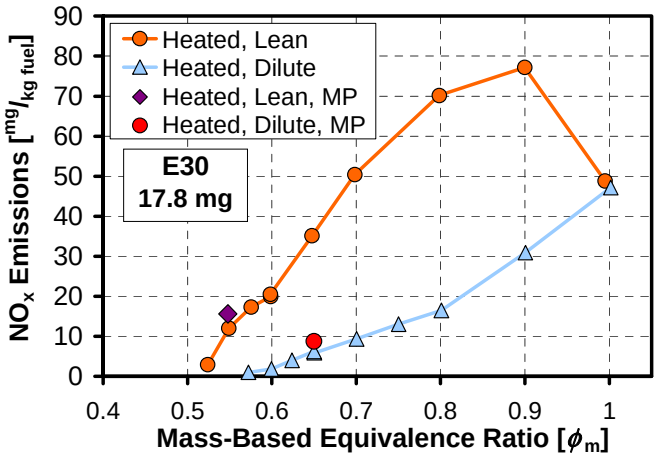

Figure 23. Fuel-specific exhaust NO_x emission as a function of ϕ_m for both lean and dilute heated operation with RS and E30 fuel. Plotted as single data points are NO_x emissions for operation with MP ignition corresponding to the E30 data in Figs. 16 and 19.

The lean ϕ-sweep shows a NO_x-emissions peak at $\phi = 0.90$, in agreement with literature [4]. For lower ϕ, NO_x emissions drop rapidly, reaching 12 mg/kg fuel at $\phi = 0.55$. Figure 8b shows that this RS data point has an $IMEP_n$ variability of 3.8%. When MP ignition is applied to induce mixed-mode combustion, the $IMEP_n$ variability drops to 2.2% (see Fig. 16), at the expense of a rise of NO_x emissions to 16 mg/kg fuel. The data point with $\phi = 0.52$ reaches as low as 2.9 mg NO_x /kg fuel, but it has an unacceptably large $IMEP_n$ variability of 8.3%. Nonetheless, such low NO_x emissions serve as a motivation for further research aimed at stable ultra-lean SI operation.

Lastly, it can be noted from Fig. 23 that the NO_x emissions are much lower for dilute stoichiometric operation for all ϕ_m lower than 1.0. Similarly to the lean case, the application of MP ignition to induce more stable mixed-mode combustion (see Fig. 19) leads to a small but substantial rise of the NO_x emissions. On the other hand, NO_x emissions are not large concern for dilute stoichiometric operation since they can be reduced cost-effectively with a conventional three-way catalyst.

Conclusions

This study encompasses a systematic examination of pathways towards higher thermal efficiency of a DISI engine operated with $IMEP_n$ near 400 kPa at 1000 rpm, contrasting the use of high-octane gasoline and E30. For effective ignition, both a conventional high-energy inductive spark system and a more powerful research-grade multi-pulse (MP) transient plasma system are used.

Several factors have been identified that affect the realized gains of thermal efficiency for well-mixed lean and dilute DISI engine operation in comparison with non-dilute stoichiometric operation.

High thermal efficiency is favored by:

1. Short delay from spark to main combustion (*i.e.* fast inflammation), which reduces cycle-to-cycle variations of the deflagration-based combustion for both lean and dilute operation.
2. Lean operation, which promotes high combustion efficiency, shorter burn duration and faster inflammation.
3. Intake gas heating, which promotes inflammation and shifts onset of combustion instability to lower ϕ or ϕ_m. It also enables mixed-mode combustion, which is characterized by a combination of deflagration and end-gas autoignition.
4. The more reactive gasoline fuel, which facilitates end-gas autoignition and enables mixed-mode combustion while not requiring an overly advanced combustion phasing.

For the conditions studied, lean gasoline operation with intake-air heating provides the highest fuel-economy gains (≈ 20%). Here, mixed-mode combustion provides a beneficial speed-up of the final combustion phase, thereby increasing the degree of constant-volume heat release and providing high work-extraction efficiency.

For lean operation with the higher-octane E30 and for dilute operation with either fuel, the RS system does not provide sufficiently strong combustion-phasing control to allow stable operation with sufficiently advanced combustion phasing to induce mixed-mode combustion. Here, the faster inflammation offered by MP ignition improves the combustion-phasing control and enables stable mixed-mode combustion. This benefits in particular heated dilute operation, for which the FE gain increases from 10% to 11.5% while $IMEP_n$ variability is reduced from 1.8 to 1.1% at $\phi_m = 0.65$ (corresponding to 35% simulated EGR).

For heated lean E30 operation, the MP ignition systems enables stable mixed-mode combustion, which was not attainable with the RS ignition system. However, the FE gain remains lower than for gasoline (17 vs. 20%), likely due to the higher octane numbers of E30 that require an overly advanced combustion phasing to induce end-gas autoignition.

The heated dilute operating point with mixed-mode combustion shows no difference in autoignition between the two fuels, despite substantially different RON and MON. This suggests that heated N_2-diluted SI operation with a combustion phasing near TDC provides end-gas conditions that are “beyond MON”, with $K > 1$.

Mixed-mode combustion with end-gas autoignition provides benefits by shortening the combustion duration for both lean and dilute operation, but it introduces a noise concern. To avoid occasional knocking cycles, mixed-mode combustion should be restricted to very lean ($\phi \leq 0.55$) or highly dilute ($\phi_m \leq 0.65$) operation, while ensuring very repeatable deflagration-based combustion that provides low cycle-to-cycle variations of the peak cylinder pressure (≤ ±3%).

References

1. IPCC, 2013: “Climate Change 2013: The Physical Science Basis. Contribution of Working Group I to the Fifth Assessment Report of the Intergovernmental Panel on Climate Change”, [Stocker, T.F., Qin, D., Plattner, G.-K., Tignor, M., Allen, S.K., Boschung, J., Nauels, A., Xia, Y., Bex, V., and Midgley, P.M. (eds.)], Cambridge University Press, Cambridge, United Kingdom and New York, NY, USA.
2. Dale, J.D., Checkel, M.D., and Smy, P.R., “Application of high energy ignition systems to engines”, Prog. Energy Combust. Sci. 23:379-98, 1997, doi: 10.1016/S0360-1285(97)00011-7.
3. Newhall, H.K., “Kinetics of Engine-generated Nitrogen Oxides and Carbon Monoxide”, Proc. Comb. Inst. 12(1):603–613, 1969, doi: 10.1016/S0082-0784(69)80441-8.
4. Heywood, J.B., Internal Combustion Engine Fundamentals, McGraw-Hill, New York, 1988.
5. Advanced Ignition Systems for Gasoline Engines, eds. Kratzsch, M., Günther, M., expert verlag, Renningen, Germany, 2013, ISBN 978-3-8169-3190-4.
6. Sjöberg, M., Zeng, W., Singleton, D., Sanders, J. et al., "Combined Effects of Multi-Pulse Transient Plasma Ignition and Intake Heating on Lean Limits of Well-Mixed E85 DISI Engine Operation," SAE Int. J. Engines 7(4):1781-1801, 2014, doi:10.4271/2014-01-2615.
7. Hall, M., Matthews, R., and Ezekoye, O., "Railplug Ignition Operating Characteristics and Performance: A Review," SAE Technical Paper 2007-01-1832, 2007, doi:10.4271/2007-01-1832.
8. Kupe, J., Wilhelmi, H., and Adams, W., "Operational Characteristics of a Lean Burn Sl-Engine: Comparison Between Plasma-Jet and Conventional Ignition System," SAE Technical Paper 870608, 1987, doi:10.4271/870608.
9. Alger, T., Gingrich, J., Mangold, B., and Roberts, C., “A Continuous Discharge Ignition System for EGR Limit Extension in SI Engines,” SAE Int J Engines, 2011;4:677-92, doi: 10.4271/2011-01-0661.
10. Yamamoto, H., Horita, S., and Matsuoka, T., "Surrounding Combustion Process (SCP) - New Concept for Lean Burn Engine," SAE Technical Paper 920058, 1992, doi:10.4271/920058.
11. Piock, W., Weyand, P., Wolf, E., and Heise, V., "Ignition Systems for Spray-Guided Stratified Combustion," SAE Int. J. Engines 3(1):389-401, 2010, doi:10.4271/2010-01-0598.
12. Zeng, W., Sjöberg, M., and Reuss, D., "Using PIV Measurements to Determine the Role of the In-Cylinder Flow Field for Stratified DISI Engine Combustion," SAE Int. J. Engines 7(2):615-632, 2014, doi:10.4271/2014-01-1237.

13. Ju, Y. and Sun, W., “Plasma assisted combustion: Dynamics and chemistry,” Prog. Energy Combust. Sci. 48:21-83, 2015, doi:10.1016/j.pecs.2014.12.002.
14. Dec, J. and Sjöberg, M., "A Parametric Study of HCCI Combustion - the Sources of Emissions at Low Loads and the Effects of GDI Fuel Injection," SAE Technical Paper 2003-01-0752, 2003, doi:10.4271/2003-01-0752.
15. Anderson, J., Leone, T., Shelby, M., Wallington, T. et al., "Octane Numbers of Ethanol-Gasoline Blends: Measurements and Novel Estimation Method from Molar Composition," SAE Technical Paper 2012-01-1274, 2012, doi:10.4271/2012-01-1274.
16. Nishio, N., Aochi, T., Yokoo, N., Nakata, K. et al., "Design of a High Ignitability Spark Plug with a Flow Guide Plate," SAE Technical Paper 2015-01-0780, 2015, doi:10.4271/2015-01-0780.
17. Middleton, R.J., Manofsky Olesky, L.K., Lavoie, G.A., Wooldridge, M.S., *et al.*, “The effect of spark timing and negative valve overlap on Spark Assisted Compression Ignition combustion heat release rate,” Proc Comb Inst 35(3):3117-3124, 2015, doi:10.1016/j.proci.2014.08.021
18. Kasseris, E. and Heywood, J., "Charge Cooling Effects on Knock Limits in SI DI Engines Using Gasoline/Ethanol Blends: Part 2-Effective Octane Numbers," SAE Int. J. Fuels Lubr. 5(2):844-854, 2012, doi:10.4271/2012-01-1284.
19. Ayala, F., Gerty, M., and Heywood, J., "Effects of Combustion Phasing, Relative Air-fuel Ratio, Compression Ratio, and Load on SI Engine Efficiency," SAE Technical Paper 2006-01-0229, 2006, doi:10.4271/2006-01-0229.
20. Personal communication with Marco Mehl, Lawrence-Livermore National Laboratory, 2015.
21. Boumehdi, M.A., Stepanyan, S.A., Desgroux, P., Vanhove, G., Starikovskaia, S.M., “Ignition of methane- and n-butane-containing mixtures at high pressures by pulsed nanosecond discharge,” Combustion and Flame 162(4):1336-1349, 2015, doi:10.1016/j.combustflame.2014.11.006
22. Kalghatgi, G., "Fuel Anti-Knock Quality - Part I. Engine Studies," SAE Technical Paper 2001-01-3584, 2001, doi:10.4271/2001-01-3584.
23. Risberg, P., Kalghatgi, G., and Ångström, H., "Auto-ignition Quality of Gasoline-Like Fuels in HCCI Engines," SAE Technical Paper 2003-01-3215, 2003, doi:10.4271/2003-01-3215.
24. Sjöberg, M. and Dec, J., "Ethanol Autoignition Characteristics and HCCI Performance for Wide Ranges of Engine Speed, Load and Boost," SAE Int. J. Engines 3(1):84-106, 2010, doi:10.4271/2010-01-0338.
25. Dec, J., Yang, Y., Dernotte, J., and Ji, C., "Effects of Gasoline Reactivity and Ethanol Content on Boosted, Premixed and Partially Stratified Low-Temperature Gasoline Combustion (LTGC)," SAE Int. J. Engines 8(3):935-955, 2015, doi:10.4271/2015-01-0813.
26. Grandin, B. and Denbratt, I., "The Effect of Knock on Heat Transfer in SI Engines," SAE Technical Paper 2002-01-0238, 2002, doi:10.4271/2002-01-0238.
27. Pauly, T., Franoschek, S., Hoyer, R., and Eckhoff, S., "Cost and Fuel Economy Driven Aftertreatment Solutions for Lean GDI," SAE Technical Paper 2010-01-0363, 2010, doi:10.4271/2010-01-0363.

Acknowledgments

The authors would like to thank Daniel Singleton at TPS Inc. for providing the special spark plug used with the multi-pulse transient plasma ignition system. Isaac Ekoto of Sandia National Laboratories made the TPS pulse generator available for these experiments. The authors would also like to thank Alberto Garcia, Gary Hubbard, Chris Carlen, Ken St. Hilaire, Keith Penney, and Sal Birtola for their dedicated support of the DISI laboratory. Mark Musculus and David Reuss provided valuable input for the manuscript. Marco Mehl at LLNL should be gratefully acknowledged for performing the chemical-kinetics calculations that produced the flame-speed data plotted in Fig. 12.

The work was performed at the Combustion Research Facility, Sandia National Laboratories, Livermore, CA. Financial support was provided by the U.S. Department of Energy, Office of Vehicle Technologies. Sandia National Laboratories is a multi-program laboratory managed and operated by Sandia Corporation, a wholly owned subsidiary of Lockheed Martin Corporation, for the U.S. Department of Energy’s National Nuclear Security Administration under contract DE-AC04-94AL85000.

Definitions/Abbreviations

ϕ	Equivalence Ratio
ϕ_{in}	Mass-based Equivalence Ratio
η_{comb}	Combustion Efficiency
η_{th}	Thermal Efficiency
°CA	Crank-Angle Degree
AHRR	Apparent Heat Release Rate
AKI	Anti-Knock Index
aTDC	after Top Dead Center
CA10	10% Burn Point
CA50	50% Burn Point
CA90	90% Burn Point
CO	Carbon Monoxide
COV of IMEP	Coefficient of Variation of IMEP
CSD of IMEP	Corrected Standard Deviation of IMEP
DISI	Direct Injection Spark Ignition
E30	Blend of Gasoline with 30% Ethanol by Volume

E85	Blend of Gasoline with 85% Ethanol by Volume
EGR	Exhaust-Gas Recirculation
FE	Fuel Economy
FWHM	Full-Width at Half-Maximum
HC	(Unburned) Hydrocarbons
$IMEP_n$	Indicated Mean Effective Pressure – net (4 strokes)
FPT	First Pulse Timing
IVC	Intake Valve Closing
LHV	Lower Heating Value
L-P	Low-Pass
MON	Motor Octane Number
m_{CO}	Mass of CO Emitted each Cycle
$m_{Injected\text{-}Fuel}$	Mass of Fuel Injected each Cycle
m_{HC}	Mass of HC Emitted each Cycle
MP	Multi-Pulse Transient Plasma
NVH	Noise, Vibration and Harshness
NO_x	Nitrogen Oxides
RON	Research Octane Number
RS	Regular Spark
SD	Standard Deviation
SACI	Spark-Assisted Compression Ignition
SI	Spark Ignition
SOI	Start of Injection
ST	Spark Timing
TDC	Top Dead Center
VCO	Valve Covered Orifice

Appendix A

To verify that the use of Eq. 4 provides a reasonable estimate of the end-gas reactant temperature, CHEMKIN-PRO was used for a more accurate computation of the temperature rise of the reactants that occurs as a result of the pressure-induced gas compression. The results are shown in Fig. A1.

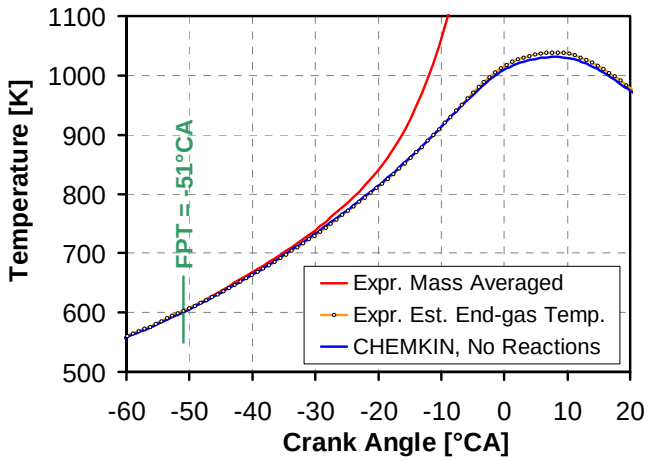

Figure A1. Comparison of end-gas temperature estimated using Eq. 4 with that computed with CHEMKIN-PRO which includes a detailed thermodynamic library. The experimentally determined mass-averaged temperature is plotted as well. E30 fuel with heated intake and ϕ = 0.55.

Figure A1 shows that the application of Eq. 4 captures well the temperature rise estimated with CHEMKIN-PRO, with a deviation of around 10K for crank angles near peak temperature. It can also be noted that the mass-averaged temperature does not deviate substantially from the end-gas reactant temperature until roughly 20°CA after ignition. This demonstrates that the heat-release rate initially is very low for lean operation with ϕ = 0.55.